

## NUMERICAL INSIGHTS INTO THE TRANSIENT BEHAVIOUR OF SINGLE PHASE NATURAL CONVECTION LOOPS FOR NUCLEAR PASSIVE COOLING APPLICATIONS

**Dean Wilson**

School of MACE

The University of Manchester  
Oxford Road, Manchester, M13 9PL  
dean.wilson@manchester.ac.uk

**Hector Iacovides**

School of MACE

The University of Manchester  
Oxford Road, Manchester, M13 9PL  
h.iacovides@manchester.ac.uk

**Tim Craft**

School of MACE

The University of Manchester  
Oxford Road, Manchester, M13 9PL  
tim.craft@manchester.ac.uk

### ABSTRACT

Natural Circulation Loops (NCLs), where fluid is driven through a closed circuit solely by thermal imbalance, offer potential for use in passive cooling systems within nuclear power plants. Transient CFD simulations of two-dimensional natural circulation loops of different aspect ratios has been performed using the Unsteady Reynolds-averaged Navier-Stokes framework for a range of Rayleigh numbers ( $8 \times 10^8 < Ra < 8 \times 10^{12}$ ) in order to provide insight into the transient behaviour of such systems. Results predict that NCL systems exhibit complex and rich dynamic behaviour, with strong sensitivity to the imposed Rayleigh number. Initial thermal transients led to the establishment of unstable and oscillatory flow behaviour which, in most cases, led to flow reversals. Cases at the lower  $Ra = 8 \times 10^8$  reached a statistically steady-state whilst flows at the higher  $Ra = 8 \times 10^{12}$  demonstrated more oscillatory, but relatively regular, behaviour.

### INTRODUCTION

The use of passive safety systems in nuclear power has been discussed since at least the mid 1980's, where it was recognized that they have the potential to contribute towards the simplification, safety and improved economics of new Nuclear Power plant designs (IAEA, 2005). As a result, these types of systems are being considered for numerous current reactor concepts, including Generation III and III+, and are also expected to play a significant role in the development of future Generation IV reactors (Gen IV International Forum, 2013).

One such system employs a *Natural Circulation Loop* (NCL), a closed circuit which exploits natural convection phenomena to intentionally transports thermal energy from a high-temperature source to a low temperature sink without recourse to pumping devices. Designed and implemented correctly, this feature of NCLs could potentially allow for essential reactor cooling to continue during a station black-

out or other severe accident scenario, without the need for any source of external power or operator intervention.

Whilst some next-generation nuclear reactors (the Westinghouse AP1000, for example) already incorporate various such passive safety systems (Wibisono *et al.*, 2013), a review by (Basu *et al.*, 2014) found only limited application of multidimensional numerical tools to NCL system within the open literature. Wang *et al.* (2013) presented 3D numerical results for a square loop with a cooler on the upper horizontal leg and a heater on the lower horizontal leg. Comparisons of global parameters ( $Re$ ,  $Gr$ ) with prior experiments by Misale *et al.* (2007) demonstrated good agreement but some discrepancies were noted when comparing the time-history of the temperature difference across the heater. A recent numerical study by Kudariyawar *et al.* (2016) provided 3D steady state and transient CFD simulations for NCLs with various configurations of heaters and coolers. Results showed good agreement with the experimental correlations of Vijayan *et al.* (1991) and demonstrated interesting transient behaviour but, as with the study by Wang *et al.*, a lack of high fidelity experimental or numerical data prevented complete validation of the three-dimensional flow and thermal fields.

The numerical modelling methodology currently favoured by the nuclear industry makes use of 'systems codes', which are typically 1D and rely heavily on empirical and scale-dependent correlations obtained via experimentation. Whilst these have been shown to provide fairly reliable predictions of integral parameters (though limited, of course, to the parameter ranges that the underlying correlations were developed for), these codes cannot be expected to reproduce the significant complex 3D local effects inherent to natural convection phenomena and which can influence the overall system behaviour. Modern general purpose multidimensional Computational Fluid Dynamics (CFD) codes have now reached a degree of maturity, and thus, if properly verified and validated, have the potential to provide detailed, reliable and accurate solutions to the kinds

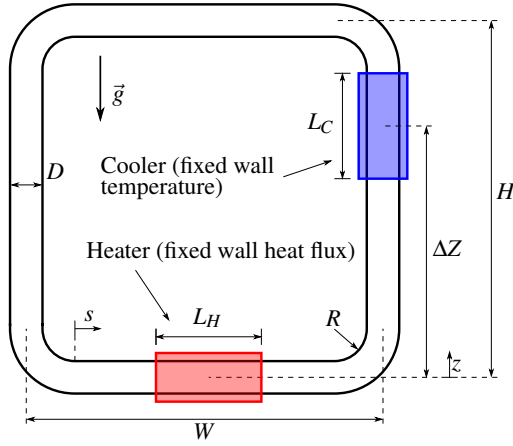


Figure 1. Geometry for a simple NCL.

Table 1. Non-dimensional geometric relations for the loop considered in Figure 1, where  $L_i$  represents  $L_C$  or  $L_H$ .

|        | $H/D$ | $H/W$ | $R/D$ | $\Delta Z/H$ | $L_i/W$ |
|--------|-------|-------|-------|--------------|---------|
| Square | 10    | 1     | 1.5   | 0.675        | 0.35    |
| Tall   | 10    | 2     | 1.5   | 0.675        | 0.35    |

of complex nuclear thermal-hydraulic problems posed by NCL systems.

This study aims to provide further insight into the complex transient behaviour of NCLs through a series of unsteady 2D numerical simulations at a range of Rayleigh numbers, and for different loop geometries. Solving in 2D allows simulations to be performed relatively quickly, and without significant computation expense, whilst still capturing a significant proportion of the flow physics. Aside from being interesting in their own right, they will also help to identify cases that might be suitable for further study using higher fidelity 3D techniques, including Large Eddy Simulation or Direct Numerical Simulation, which can in turn drive RANS development by providing valuable validation data. The simulations also aim to further demonstrate the potential of the Unsteady Reynolds-Averaged Navier-Stokes (URANS) framework in resolving complex transient flows and natural convection phenomena.

## CASE SET-UP

At their most basic, a NCL consists of a closed circuit with both a source and sink of thermal energy, positioned with some elevation difference between them. A number of possible configurations exist, differing mainly in the arrangement and orientation of the thermal source and sink.

In this study, a geometrically simple NCL system is considered, comprising a two-dimensional (planar) loop with a horizontal oriented heater and a vertical oriented cooler. Two loop geometries are considered, differing only in their aspect ratio and in the positioning of the vertical cooler. A schematic is shown in Figure 1, with corresponding dimensional relations provided in Table 1. The heater provides a constant heat flux whilst the walls of the cooler are maintained at a fixed temperature. Adiabatic and no-slip conditions are set for the remainder of the loop.

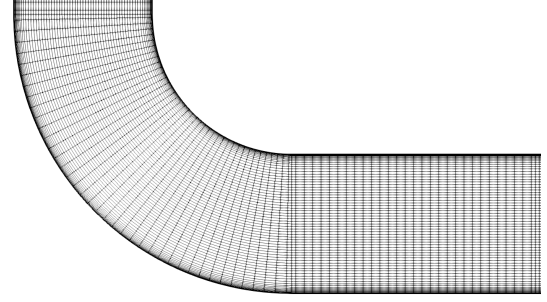


Figure 2. Close up of the bottom left elbow of the low- $Re$  mesh generated for  $Ra = 10^8$ .

## Flow specification

Following the non-dimensional analysis proposed by Vijayan (2002), the flow conditions are specified using a Rayleigh number based on a modified Grashof number.

$$Ra_m = Gr_m \cdot Pr, \quad Gr_m = \frac{D^3 \rho^2 \beta g \Delta T_r}{\mu^2} \quad (1)$$

where  $D$  is the loop hydraulic diameter,  $\rho$  is the fluid density,  $\beta$  is the fluid volume expansion coefficient,  $g$  is acceleration due to gravity, and  $\mu$  is the fluid viscosity. The Prandtl number is  $Pr = 0.71$  and the reference temperature difference,  $\Delta T_r$ , is defined as

$$\Delta T_r = \frac{Q_h \Delta Z}{A \mu C_p} \quad (2)$$

where  $Q_h$  is the total heat input rate into the heater,  $\Delta Z$  is the height difference between the heater and cooler, and  $A$  is a reference cross-sectional area. Three different Rayleigh numbers are considered for both loop sizes:  $Ra = 8 \times 10^8$ ,  $8 \times 10^{10}$  and  $8 \times 10^{12}$ .

By further assuming a steady state exists, and by utilizing friction factors for laminar and turbulent flow, Vijayan (2002) proposed a correlation relating the modified Grashof number (as the primary input) to the steady state Reynolds number of the flow around the loop (as the output)

$$Re_{SS} = C \left( \frac{Gr_m}{N_G} \right)^r \quad (3)$$

where  $Re_{SS} = D \dot{m}_{SS} / A \mu$  and  $N_G = L_t / D$  is a geometric parameter which non-dimensionalises the length of the loop. With suitable values of the constants  $C$  and  $r$ , Equation 3 provides both a means to compare steady-state flow conditions across different loops (if such a steady-state exists) and compute characteristic quantities which can be used to non-dimensionalise results (e.g. a steady-state mass flow rate,  $\dot{m}_{SS}$ , and temperature rise across the heater,  $(\Delta T_h)_{SS} = Q_h / \dot{m}_{SS} C_p$ ). Vijayan (2002) proposed  $C = 0.1768$ ,  $r = 0.5$  for laminar flow and  $C = 1.96$ ,  $r = 1/2.75$  for turbulent flow.

## Numerical modelling

The Launder & Sharma (1974) low- $Re$  variant of the  $k - \epsilon$  model is used for the turbulence and the simple gradient diffusion hypothesis is used for the turbulent heat flux.

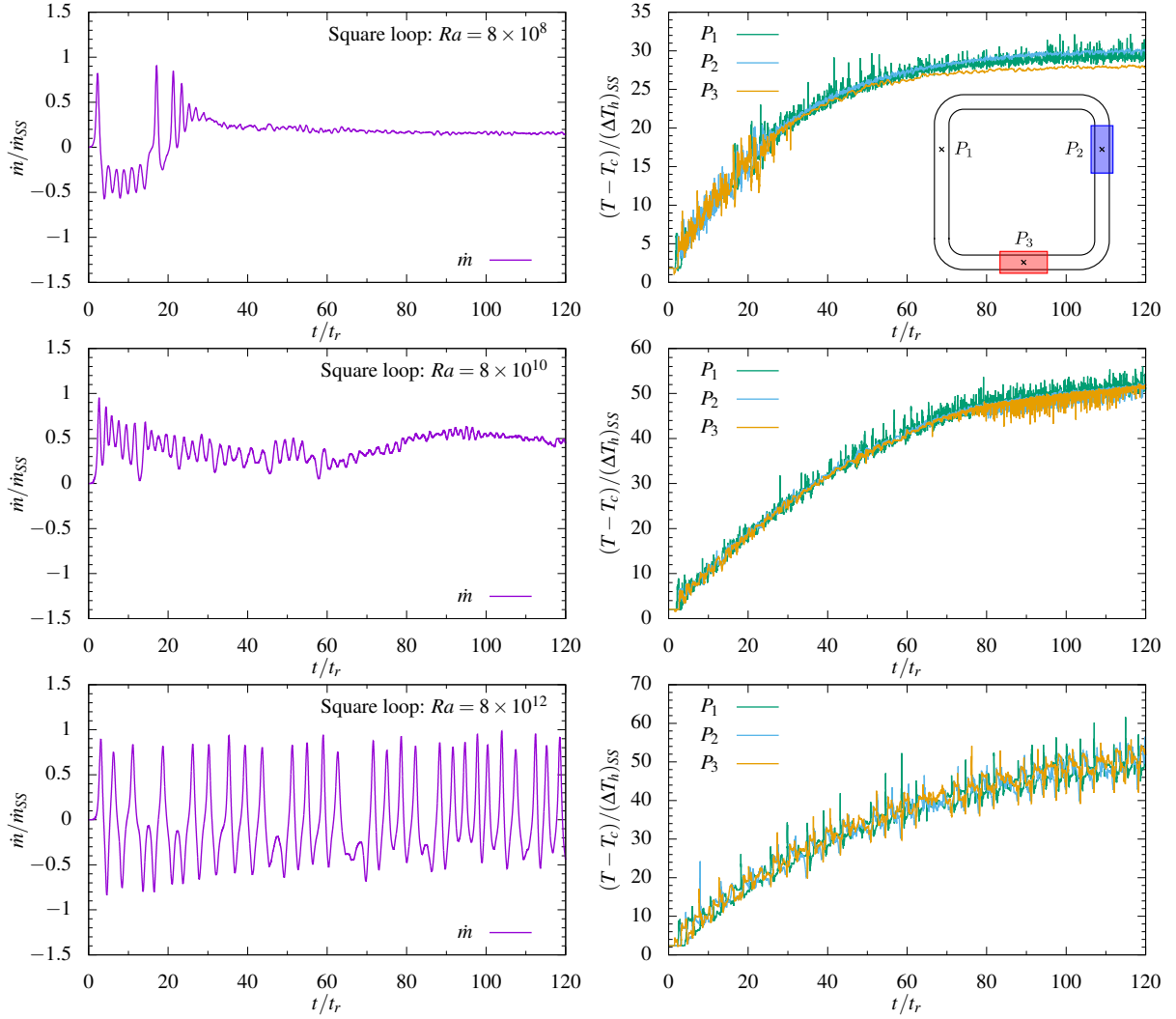


Figure 3. Mass flow rate (left) and temperature monitors (right) at the points indicated inset for the square loop at (from top to bottom)  $Ra = 8 \times 10^8$ ,  $8 \times 10^{10}$ ,  $8 \times 10^{12}$ . A positive  $\dot{m}$  indicates clockwise flow.

The effects of buoyancy are incorporated by utilizing the Boussinesq approximation, which assumes that density differences are small enough to be neglected in the inertial terms and only become significant when multiplied by acceleration due to gravity. Density variations are incorporated by assuming a linear dependence with temperature.

Block structured meshes comprising hexahedral elements are utilized with a low- $Re$  approach (i.e. with  $y^+ \approx 1$ ) applied for all Rayleigh numbers considered. After mesh sensitivity tests, meshes with total cell counts of between  $N = 40128$  (square case at  $Re_m = 8 \times 10^8$ ) and  $N = 134481$  (tall case at  $Re_m = 8 \times 10^{12}$ ) were produced using the meshing package ANSYS ICEMCFD (v19.2). A close up image of the lower left corner of the mesh produced for  $Ra = 10^8$  is presented in Figure 2.

To provide a suitable value for the time-step, a reference time-scale is constructed by considering the loop circulation time  $t_r = V_t \rho / \dot{m}_{SS}$ , where  $V_t$  is the total volume of the loop and  $\dot{m}_{SS}$  is a mass flow rate obtained from a  $Re_{SS}$  predicted by the Equation 3. Owing to the expectation that a considerable amount of local unsteady behaviour will be present, we chose to resolve a single circulation in approximately 10000 steps. After further time-step sensitivity tests, this corresponded to a range of time steps from  $\Delta t = 0.005$  (square case at  $Ra_m = 8 \times 10^8$ ) to  $\Delta t = 0.001$  (tall case at

$Re_m = 8 \times 10^{12}$ ).

The flows are solved using our in-house structured finite-volume solver STREAM running in unsteady mode, which solves the usual equations of mass, momentum and energy in addition to those of the turbulence model. All simulations begin from stagnant conditions to enable the initial transient evolution of the flow to be captured. The initial bulk temperature of the fluid was specified to be very close to the fixed temperature assigned to the cooler walls ( $T_c$ ).

## RESULTS

### Square loop

Figure 3 presents time-history plots of non-dimensional mass flow rate and temperature for the square case at the three  $Ra$  considered. Results show that the flow in the loops exhibits significant start-up transients which lead to both oscillatory behaviour and, in some cases, flow reversals. At  $Ra = 8 \times 10^8$  the flow initially travels clockwise around the loop before arresting and then reversing direction. A series of flow reversals, interspersed with more oscillatory changes in the mass flow rate, can be seen before the flow appears to settle into a statistically steady-state. The temperature monitors, on the right of Figure 3, show that the bulk temperature in the loop rises

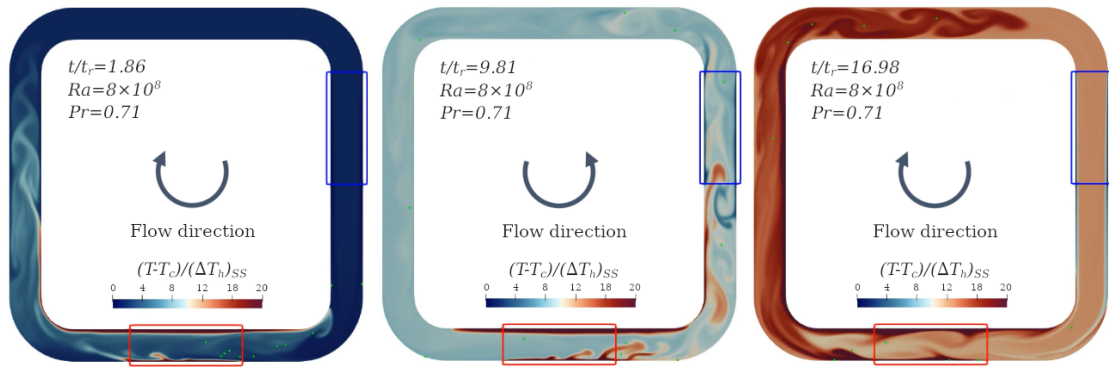


Figure 4. Selected snapshots showing instantaneous contours of non-dimensional temperature for the square loop at  $Ra = 8 \times 10^8$ . A flow field animation for this case can be found at <https://sites.manchester.ac.uk/thermofluids/research/>.

over time for all  $Ra$  considered, indicating the heat flux provided by the heater is initially dominant. As the heat flux out of the cooler rises, however, the change in bulk temperature reduces towards zero. A clockwise flow direction is implied by the arrangement of heater and cooler considered in this NCL (at steady-state) since whilst the horizontally oriented heater does not offer a preferential direction, the vertical cooler does.

At  $Ra = 8 \times 10^{10}$  the mass flow rate plot reveals less coherent behaviour, despite temperature monitors showing similar overall thermal changes between cases, with no flow reversals and indeterminate oscillations. At  $Ra = 8 \times 10^{12}$  the flow displays more periodic behaviour. Continual flow reversals are seen, interspersed with occasional ‘half’ reversals, where the flow initially slows towards zero before accelerating again without changing direction. Unlike at the lower  $Ra$ , the amplitude of the oscillations in the mass flow rate does not appear to be significantly reducing. Further simulation would be required to determine the stability of this flow pattern.

To elucidate the intriguing behaviour discussed above Figure 4 presents a series of instantaneous snapshots of non-dimensional temperature for the square loop at  $Ra = 8 \times 10^8$ . Initially, the heat flux imparted to the fluid in the heater leads to the production of a number of buoyant plumes. These rise within the heater section of the pipe and impinge on the upper heater surface, where they travel left and right in almost equal measure. Since, as indicated earlier, the initial heat flux provided by the heater is significantly higher than the outgoing heat flux within the cooler, the cooler does not cool the fluid enough to produce an equivalent effect in the right leg. The hot fluid can then be seen to rise up the left hand leg (Figure 4 left) where, since the left leg is now less dense on average than the right leg, clockwise circulation of the fluid is initiated. The inertia imparted to the fluid by this circulation then takes the hot fluid ‘plug’ around the top leg and into the right leg, drawing the colder fluid from the right leg through the heater. Since, in this case, the fluid passes through the heater too quickly for it to significantly reduce in density, the denser fluid now present in the left leg causes the flow to reverse direction and circulation commences in an anti-clockwise direction.

The above description forms the basic physical mechanism for the reversals and oscillatory behaviour; any imbalance between the average densities in the left and right vertical legs will lead to a resultant buoyancy force, either slowing or accelerating the fluid. Changes in the density

(temperature) imbalance, and thus the resultant flow rate, are affected by the two dissipation mechanisms (viscous and thermal) and the two external sources of heat transfer (heater and cooler), which will themselves impose different thermal time scales owing to differences in the thermal boundary conditions. If any of these effects are out of phase, then overshooting may occur and instabilities may grow. In the cases considered here, this manifests in the form of oscillatory flow behaviour and flow reversals.

### Tall loop

Results of simulations with the taller loop, presented in Figure 5, predict unstable and dynamic behaviour not dissimilar to the square loop. Time-history monitors of temperature and mass flow rate for  $Ra = 8 \times 10^8$  shows almost identical behaviour, with flow reversals predicted at similar times but slightly different peak mass flow rates. Results at  $Ra = 8 \times 10^{12}$  also show comparable behaviour, with the mass flow rate monitors revealing a very regular pattern of flow reversals, albeit with noticeably smaller periods and larger peak amplitudes to that predicted in the square loop. The increased vertical distance over which the buoyancy force can act (and thus larger column of fluid which can initiate motion) clearly contributes towards these differences.

More significant differences can be seen between the two geometries at  $Ra = 8 \times 10^{10}$ , however. Whilst results with the square loop indicated more irregular behaviour in the mass flow rate, results with the tall loop show that the flow appears to somewhat settle after an initial flow reversal but travels counter-clockwise, in opposition to what might be expected. Oscillations in the mass flow rate then grow in amplitude before another flow reversal occurs. The flow does then settle in statistically steady state, in contrast with the predictions in the square loop at this  $Ra_m$ .

### Steady-state behaviour

As discussed in the previous section, only a subset of the cases considered have reached a statistically steady-state within the time period considered here. For the square case at  $Ra = 8 \times 10^8$ , results were time-averaged after the flow appeared to reach a statistically steady state. Long-term time-averaged contours of non-dimensional temperature are presented for this case in Figure 6 and predict an interesting flow feature in the lower right elbow. Warmer fluid from the heater leaks around the upper surface of the lower right elbow, on average, leading to impingement against the cooler fluid sinking down the right leg from the cooler. This diver-

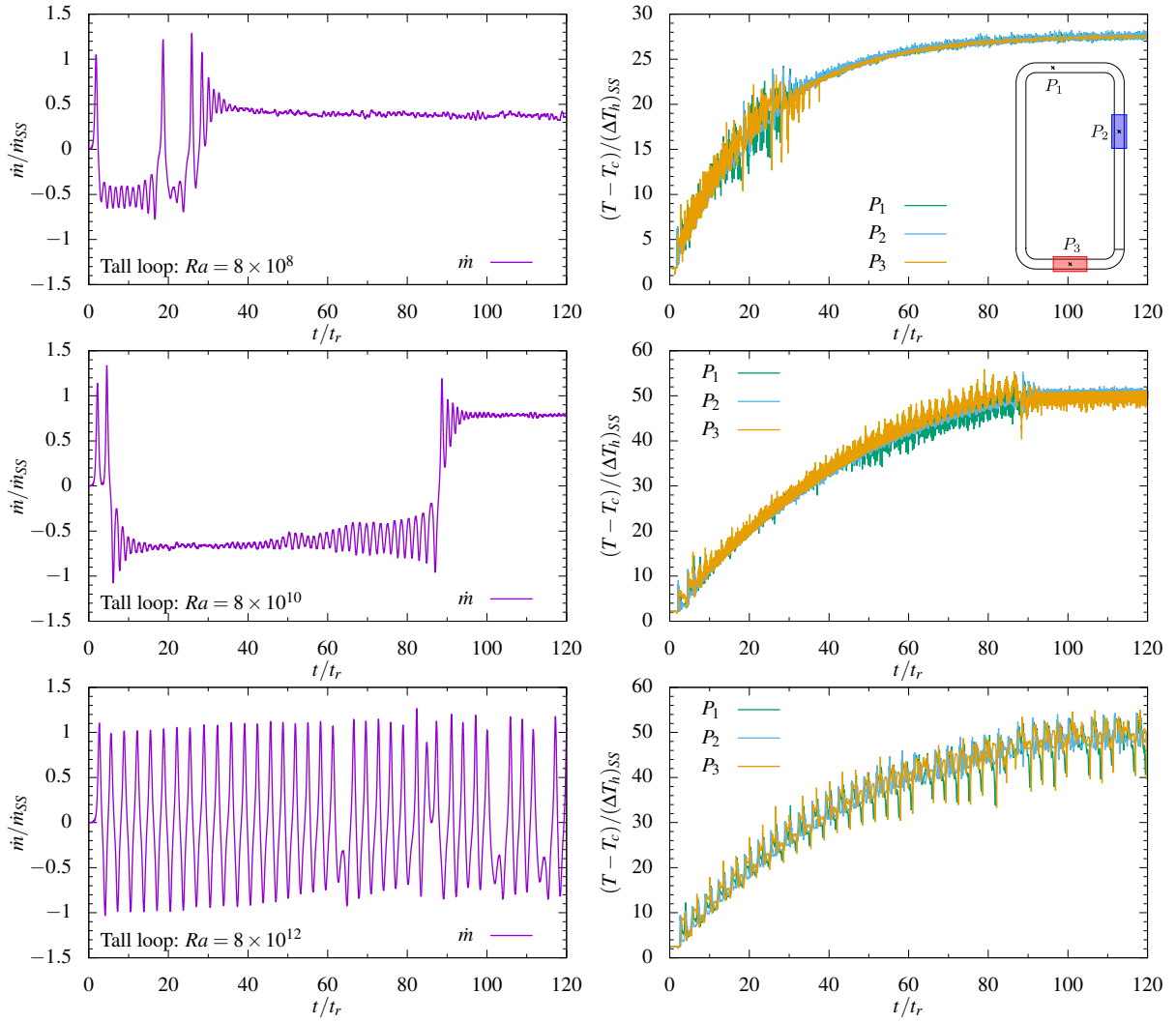


Figure 5. Mass flow rate (left) and temperature monitors (right) at the points indicated inset for the tall loop at (from top to bottom)  $Ra = 10^8, 10^{10}, 10^{12}$ . Positive  $\dot{m}_{SS}$  indicates clockwise flow.

sion causes the flow profile to meander slightly as it navigates the lower right corner before straightening up after it passes through the heater. Corresponding long-term time-averaged results for the tall loop (not shown) do not reveal such a feature.

### Comparisons with existing correlations

In order to provide some limited quantitative assessment of the flow predictions, the steady-state Reynolds number,  $Re_{SS}$ , obtained for a given  $(Gr_m/N_G)$  input combination, is plotted in Figure 7. Only those cases which have reached a statistically steady-state have been included and comparisons are drawn both against data compiled by Vijayan (2002) for a wide range of experimental NCLs, and the correlation in Equation 3.

Whilst all present simulations plotted tended to predict lower  $Re_{SS}$  than the correlations suggest, something particularly noticeably for the square  $Ra = 8 \times 10^8$  case considered, the comparisons do indicate that the correct trend is being reproduced as the  $Gr_m/N_G$  parameter combination changes (i.e. as  $Ra_m$  increases). Additionally, variations in the (normalized) mass flow rate for all cases considered, as per Figure 3 and 5, are of order 1, indicating broad order-of-magnitude agreement with the correlations.

Exact quantitative agreement can not be expected due to the two-dimensional planar nature of the cases simulated in this study; all experimental data plotted in Figure 7 represent NCLs with pipes and pipe geometry is also implied in the derivation of the correlation used (Vijayan, 2002).

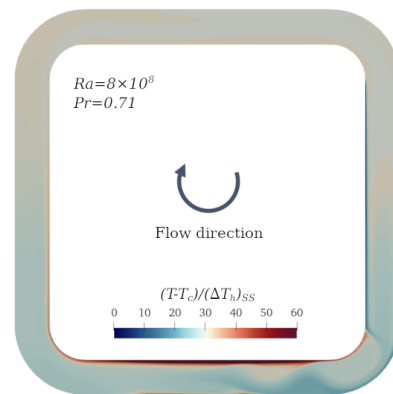


Figure 6. Selected snapshots showing instantaneous contours of non-dimensional temperature at  $Ra = 10^{10}$ . The colour map has been scaled to highlight details in the bulk of the flow; the maximum at the top heater wall is 110.14.

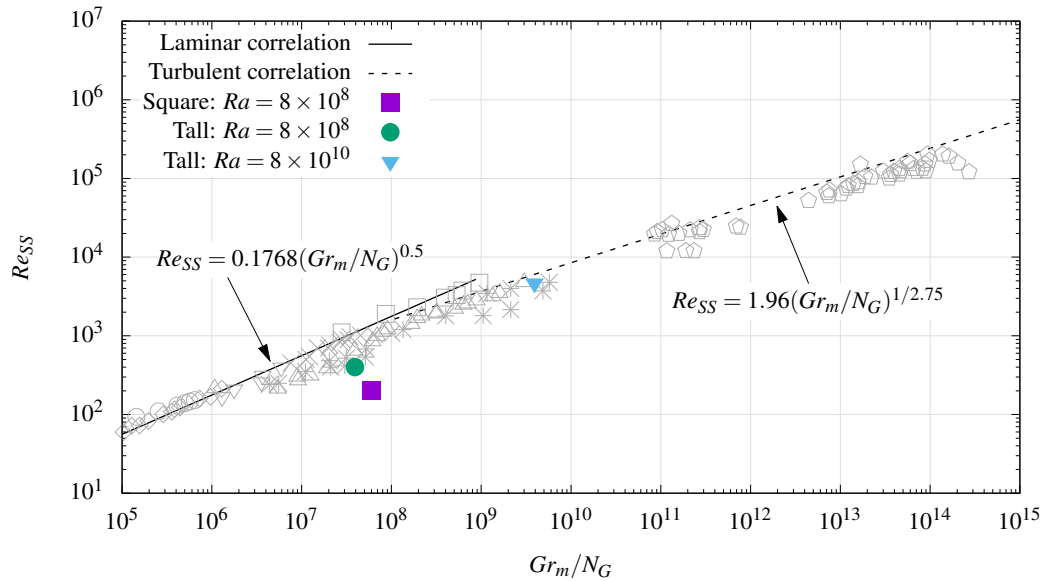


Figure 7. Comparison of resultant Reynolds number with correlations of Vijayan (2002) as defined by Equation 3 and with constants as indicated inset. Grey symbols represent data points from experimental data compiled and presented as per Vijayan (2002). Only simulations which reached a statistically steady-state have been plotted.

## CONCLUSION

CFD simulations of a single-phase natural circulation loop (NCL) have been presented with the aim of providing insight into the complex transient natural convection phenomena predicted to occur. NCLs have relevance to passive cooling systems which are increasingly being utilized by next generation reactor designers. Two relatively simple 2D loops were examined, differing in aspect ratio. A heater was placed on the lower horizontal leg and a cooler on the right vertical leg. Transient computations covered a range of Rayleigh numbers ( $8 \times 10^8 < Ra_m < 8 \times 10^{12}$ ).

Results predict initial thermal transients which lead to the establishment of unstable and oscillatory flow behaviour. This is attributed to differences between time scales associated with the thermal and momentum fields and leads, in some cases, to the prediction of flow reversals. Examination of the mass flow rate time history for each case reveals that changes to the imposed  $Ra_m$  can lead to considerable differences in predicted flow behaviour. Flows in both loop geometries at  $Ra_m = 8 \times 10^8$  were initially oscillatory but transitioned to a statistically steady-state, whilst both cases at  $Ra_m = 8 \times 10^{12}$  predicted almost continuous flow reversals. Further computations are required to establish whether or not this flow pattern is stable in the long-term. Results at  $Ra_m = 8 \times 10^{10}$  displayed greater differences; the tall geometry eventually settled into a statistically steady-state after flowing in a direction opposite to expectations whilst the flow in the square loop presented more irregular behaviour.

Overall, the results provide a number of insights into the predicted behaviour of NCLs, illustrating a rich variety of dynamic behaviour and strong sensitivity to imposed thermal conditions ( $Ra_m$ ). A number of further computations are planned, including a continuation of those cases considered presently that have not reached a statistically steady-state, the exploration of different heater and cooler configurations, and fully three-dimensional loop geometries.

## REFERENCES

- Basu, D. N., Bhattacharyya, S. & Das, P. K. 2014 A review of modern advances in analyses and applications of single-phase natural circulation loop in nuclear thermal hydraulics. *Nuclear Engineering and Design* **280**, 326–348.
- Gen IV International Forum 2013 Technology Roadmap Update for Generation IV Nuclear Energy Systems. *Tech. Rep.*
- IAEA 2005 Natural Circulation in Water Cooled Nuclear Power Plants. *Tech. Rep.* IAEA-TECDOC-1474.
- Kudariyawar, J. Y., Vaidya, A. M., Maheshwari, N. K. & Satyamurthy, P. 2016 Computational study of instabilities in a rectangular natural circulation loop using 3D CFD simulation. *International Journal of Thermal Sciences* **101**, 193–206.
- Lauder, B. & Sharma, B. 1974 Application of the energy-dissipation model of turbulence to the calculation of flow near a spinning disc. *Letters in Heat and Mass Transfer* **1** (2), 131–137.
- Misale, M., Garibaldi, P., Passos, J. C. & de Bitencourt, G. Ghisi 2007 Experiments in a single-phase natural circulation mini-loop. *Experimental Thermal and Fluid Science* **31** (8), 1111–1120.
- Vijayan, P. K. 2002 Experimental observations on the general trends of the steady state and stability behaviour of single-phase natural circulation loops. *Nuclear Engineering and Design* **215** (1), 139–152.
- Vijayan, P. K., Mehta., S. K. & Date, A. W. 1991 On the steady-state performance of natural circulation loops. *International Journal of Heat and Mass Transfer* **34** (9), 2219–2230.
- Wang, J. Y., Chuang, T. J. & Ferng, Y. M. 2013 CFD investigating flow and heat transfer characteristics in a natural circulation loop. *Annals of Nuclear Energy* **58**, 65–71.
- Wibisono, A. F., Ahn, Y., Williams, W. C., Addad, Y. & Lee, J. I. 2013 Studies of various single phase natural circulation systems for small and medium sized reactor design. *Nuclear Engineering and Design* **262**, 390–403.